A 2D weakly-coupled and efficient numerical model for transient shallow flow and movable bed

C. Juez[a,*], J. Murillo[a], P. García-Navarro[a]

[a]*LIFTEC, CSIC-Universidad de Zaragoza, Spain*

Abstract

Recent advances in free surface flows over mobile bed have shown that accurate and stable results in realistic problems can be provided if an appropriate coupling between the shallow water equations (SWE) and the Exner equation is performed. This coupling can be done if using a suitable Jacobian matrix. As a result, faithful numerical predictions are available for a wide range of flow conditions and empirical bed load discharge formulations, allowing to investigate the best option in each case study, which is mandatory in these type of environmental problems. When coupling the equations, the SWE are considered but including an extra conservation law for the sediment dynamics. In this way the computational cost may become unfordable in situations where the application of the SWE over rigid bed can be used involving large time and space scales without giving up to the adequate level of mesh refinement. Therefore, for restoring the numerical efficiency, the coupling technique is simplified, not decreasing the number of waves involved in the Riemann Problem but simplifying their definitions. The effects of the approximations made are tested against experimental data which include transient problems over erodible bed. The simplified model is formulated under a general framework able to insert any desirable discharge solid load formula.

Keywords: Finite volume method, 2D Shallow water, Bed load sediment transport, Exner equation
2000 MSC: 65N06,76B15,76M20,76N99

---

*Corresponding author
Email address: carmelo@unizar.es (C. Juez)

Manuscript accepted in *Advances in Water Resources* *March 20, 2014*

1. Introduction

The study of sediment transport is focused on the crossed relation between the moving water and the sediment materials. Despite having been analyzed since the 1950s and being widely employed in real-life engineering [1, 2], the develop of sediment transport modeling remains at present a relevant issue within the framework of the environmental modeling.

It is generally accepted that two of the fundamental concerns in modern sediment hydraulic engineering practice is the need for accurate and, in the same level of importance, efficient schemes for computing the shallow water equations together with the movement of sediment particles. The numerical strategy proposed must mimic the principal phenomenae observed in the flow field and in the movable bed.

In the search for capturing this physically significant processes Hudson et al., [3, 4] studied the influence of steady and unsteady approaches in the mathematical model when computing free surface flows considering a bed-load transport. It was commanded to consider the unsteady system contrary to what was assumed in earlier works [5, 6]. Ignoring unsteady hydrodynamical effects means that the time scales of the morphodynamics changes are smaller in comparison with the morphodynamic ones and only nearly steady process where the bed changes are generated in a slow way could be computed.

Focusing on the numerical techniques employed for obtaining the solution, a classification between asynchronous and synchronous strategies can be established [7]. Asynchronous procedures imply that the changes in the bed level are not of enough importance for affecting the hydrodynamic equations during a computational time step. This way, the continuity and momentum equations for the fluid phase are decoupled of the sediment continuity equation. They are also known as uncoupled models. On the other hand, numerical methods which solve at the same time step the hydrodynamic and morphodynamic equations are called synchronous and also, coupled. De Vriend [5] justified that asynchronous/uncoupled techniques were only valid for a limited range of hydrodynamic regimes governed by low Froude numbers and weak interactions between the flow and bed dynamics. For this reason, other authors, [8, 9, 10, 11, 12], have studied synchronous/coupled procedures, able to handle a wider range of hydrodynamic and morphodynamic situations. In some of those previous works, despite considering an extra equation for computing the sediment dynamics no additional conditions to the classical Courant-Friedrichs-Lewy (CFL) were provided for controlling the numerical stability. In particular, the lack of knowledge of an automatic numerical stability condition in [13] has driven to calibrate, by trial and error a CFL condition for obtaining a stable solution to each particular case.

In order to overcome the challenge when building a self-stable numerical scheme, several strategies have been proposed in order to derive the eigenvalues, which are responsible of the numerical stability. Ones are based on the development of the exact [14, 15, 16] or approximate form [17] of the eigenvalues of the coupled Jacobian matrix derived through the mathematical model. Other strategies are based in the numerical treatment of the whole set of equations [3, 4]. This work is focused on this last idea. In [3, 4] thanks to the Riemann theory and using a Roe's approximate Jacobian matrix of the whole system of equations was developed. Hence, the hydrodynamic and morphodynamic equations were not only solved at the same time step but also the wave celerities, which participate in the stability condition, incorporated information from both phases: water and sediment. The term coupled-Jacobian will be used for that model from now on. The main drawback of this Jacobian matrix was a strong dependence on the bed reference level. Additionally, this Jacobian matrix included the definition of the sediment transport formula through the Grass law, [18]. This formula is based in a power law of the velocity, which is nicely differentiable, and in a global calibration parameter, which is unique for all the computational domain and must be tuned in each particular problem.

Following with the Jacobian-coupled strategy, other schemes have been proposed and extended to 2D triangular meshes more recently. In [19] the identification of the approximate Jacobian matrix was achieved by means of the distribution theory [20]. However, this numerical technique needs to select families of paths that cannot be generalized. In [21] a first order HLLC scheme was proposed and a novel wave-speed estimator was provided for the Exner equation. The results were affected by numerical diffusion and a fine mesh was required by obtaining accurate results. The work in [22] described a Roe solver for a two-phase problem where the attention was devoted to the non-linear relations between primitive and conserved variables. Only the 1D approach of the problem was studied. In [23] and [24] high order and second order numerical techniques, respectively, were applied over fixed and mobile beds. However, the computational cost of such schemes was not addressed.

In [25] a novel coupled-Jacobian model was proposed and the Jacobian matrix was built with independence of the bed level reference. Regarding the calibration coefficient of Grass law, the uniqueness of this parameter in all the problem was avoided, [25, 26], by writing the law in terms of a wide number of bed-load sediment transport formulae. Although the numerical scheme of [25] was tested and verified in [26] against several experimental cases, leading to accurate and robust solutions, its applicability to a real situation, where the domain contains kilometers of river and several types of sediment, is in somehow limited by the computational cost, which is prohibitively expensive. The computational time is highly penalized by the number of algebraic operations need for computing the eigenvectors and eigenvalues of the augmented Jacobian matrix. In order to overcome this huge numerical effort in [27] a partially coupled model was proposed, although the quality of the results were compromised by the poor sediment transport law employed. Furthermore, no clear evidence of the effect of the bed wave speed in the time step restriction was provided.

Following the previous effort made by the authors, mentioned above, the main concern of this work is focused on studying a weakly-coupled way of modeling the hydrodynamic and morphodynamic 2D equations, leading to obtain a stable, generalizable and efficient numerical scheme able to run on unstructured triangular meshes. The bed-load formula employed for computing the solid discharge is the Smart-CFBS, which in [26] obtained the best agreement against experimental data and under a wide range of hydrodynamic and morphodynamic situations. The work is outlined as follows: Section 2 describes the mathematical model while in Section 3 the numerical strategy is explained. Section 4 shows the numerical results obtained, validated against 1D and 2D experimental test cases. In Section 5 conclusions arising from the work are pointed out.

2. Mathematical model

The relevant formulation of the model is based on the conservation laws applied over an infinitesimal part of the domain and evaluated on the fluid layer and to the sediment layer. The resulting system of equations is written here by means of the depth averaged shallow water equations and by the Exner equation.

2.1. Hydrodynamic model

Whether the diffusion of momentum term associated to viscosity and turbulence is omitted as well ass the Coriolis and wind effects, then the two-dimensional SWE can be expressed as in [28]:

$$\frac{\partial \mathbf{U}}{\partial t} + \frac{\partial \mathbf{F}(\mathbf{U})}{\partial x} + \frac{\partial \mathbf{G}(\mathbf{U})}{\partial y} = \mathbf{S}\left(\mathbf{U}, x, y\right) \tag{1}$$

where

$$\mathbf{U} = (h,\ q_x,\ q_y)^T \tag{2}$$

are the conserved variables with h being the water depth, $q_x = hu$ and $q_y = hv$, with (u, v) the depth averaged components of the velocity vector $\mathbf{u}$ along the (x, y) coordinates respectively. The advection terms of the above variables are expressed as:

$$\mathbf{F} = \left(q_x,\ \frac{q_y^2}{h} + \frac{1}{2}gh^2,\ \frac{q_x q_y}{h}\right)^T, \qquad \mathbf{G} = \left(q_y,\ \frac{q_x q_y}{h},\ \frac{q_y^2}{h} + \frac{1}{2}gh^2\right)^T \tag{3}$$

where g is the gravity vector. The source terms of (1) are written as

$$\mathbf{S} = \left(0,\ \frac{p_{b,x}}{\rho_w} - \frac{\tau_{b,x}}{\rho_w},\ \frac{p_{b,y}}{\rho_w} - \frac{\tau_{b,y}}{\rho_w}\right)^T \tag{4}$$

which express the x-component and y-component of: i) the term associated to the pressure force $p_{b,x}$ and $p_{b,y}$, being ρ_w the water density, that in differential form are expressed as a function of the bed slope, $\mathbf{S_o}$

$$\begin{array}{ll} \frac{p_{bx}}{\rho_w} = ghS_{o,x} & S_{o,x} = -\frac{\partial z}{\partial x} \\ \frac{p_{by}}{\rho_w} = ghS_{o,y} & S_{o,y} = -\frac{\partial z}{\partial y} \end{array} \tag{5}$$

and ii) the bed shear-stress, $\tau_{b,x}$ and $\tau_{b,y}$, that in this work is computed through the well-known Manning-Strickler's coefficient n,

$$\begin{array}{ll} \frac{\tau_{b,x}}{\rho_w} = ghS_{f,x} & S_{f,x} = \frac{n^2 u\sqrt{u^2+v^2}}{h^{4/3}} \\ \frac{\tau_{b,y}}{\rho_w} = ghS_{f,y} & S_{f,y} = \frac{n^2 v\sqrt{u^2+v^2}}{h^{4/3}} \end{array} \tag{6}$$

System (1) depends on time, is not a linear problem and additionally is non-homogeneous due to the presence of source-terms. The pure shallow water model is hyperbolic since the eigenvalues of its Jacobian matrices are always real. The presence of the source-terms leads to a non-strictly hyperbolic system. However, it is assumed that under the hypothesis of dominant advection it can be classified and numerically treated as an hyperbolic systems.

Hence, from system (1) is possible to define a Jacobian matrix, $\mathbf{J_n}$ based on the flux normal to a direction given by the unit vector, $\mathbf{n}$, $\mathbf{E_n} = \mathbf{F}n_x + \mathbf{G}n_y$, defined as

$$\mathbf{J_n} = \frac{\partial \mathbf{E_n}}{\partial \mathbf{U}} = \frac{\partial \mathbf{F}}{\partial \mathbf{U}} n_x + \frac{\partial \mathbf{G}}{\partial \mathbf{U}} n_y \tag{7}$$

whose components are

$$\mathbf{J}_n = \begin{pmatrix} 0 & n_x & n_y \\ (g_z h - u^2)n_x - uvn_y & vn_y + 2un_x & un_y \\ (g_z h - v^2)n_y - uvn_x & vn_x & un_x + 2vn_y \end{pmatrix} \tag{8}$$

The eigenvalues of this Jacobian matrix ($\lambda_1 = \mathbf{un} - c$, $\lambda_2 = \mathbf{un}$ and $\lambda_3 = \mathbf{un} + c$, with $c = \sqrt{gh}$) constitute the wave speeds in the linearized problem and provide information about directions in which the information travels.

2.2. Morphodynamic model

Sediment dynamics are assumed to be well modeled through the Exner equation [29] where sediment continuity is achieved imposing that the flux of solid transport crossing through the boundaries of the mentioned volume is the responsible of the temporal bed evolution. The Exner equation has a limit of applicability because it is based on severe assumption regarding the concentration of sediments as it was justified earlier in [30] and more recently in [31]. This point has to be retained in mind for practical simulation in order to address suitable environmental situations. Nevertheless, it is assumed that for the problems studied in this work is perfectly valid. Moreover, we are focused on the bed load transport and therefore the suspended transport is neglected driving to obtain the following expression,

$$\frac{\partial z}{\partial t} + \xi \frac{\partial q_{s,x}}{\partial x} + \xi \frac{\partial q_{s,y}}{\partial y} = 0 \tag{9}$$

where z represents the bed level, $\xi = \frac{1}{1-p}$, p takes into account the material porosity, $q_{s,x}$ and $q_{s,y}$ are the terms which compute the solid transport discharge in both directions, (x, y).

The formulation of the bed load discharge, q_s, assumes an instantaneous adaptation of the flow transport capacity to the hydrodynamic conditions, and following [25], is based on Grass law [18],

$$q_{s,x} = A_g u \left(u^2 + v^2\right) \qquad q_{s,y} = A_g v \left(u^2 + v^2\right) \tag{10}$$

where the constant A_g can be written by means of several empirical formulae as in [25, 26].

Despite of the fact that the Exner equation is not actually hyperbolic, it is possible to write a wave speed estimation associated to the sediment flux as follows

$$\lambda_b = \xi \frac{\partial \mathbf{q_{sn}}}{\partial z} \tag{11}$$

This wave speed is not related to the speed of waves having significant impact on the bed evolution in the linear analysis of the coupled-Jacobian problem [17], but instead it represents a numerical celerity to be taken into account for the stability of the uncoupled numerical solver, [12], and for the basis of the upwind strategy that is explained in the following sections.

3. Numerical model

3.1. Finite Volume Model

Initially system (1) and equation (9) are integrated in a grid cell Ω_i

$$\frac{\partial}{\partial t} \int_{\Omega} \mathbf{U} d\Omega + \int_{\Omega} (\overrightarrow{\nabla} \mathbf{E}) d\Omega = \int_{\Omega} \mathbf{S} d\Omega \tag{12}$$

$$\frac{\partial}{\partial t} \int_{\Omega} z d\Omega + \int_{\Omega} \xi (\overrightarrow{\nabla} \mathbf{q_s}) d\Omega = 0 \tag{13}$$

Using Gauss theorem (12) and (13) are written as

$$\frac{\partial}{\partial t} \int_{\Omega_i} \mathbf{U} d\Omega + \oint_{\partial\Omega_i} \mathbf{E_n} dl = \int_{\Omega_i} \mathbf{S} d\Omega \tag{14}$$

$$\frac{\partial}{\partial t} \int_{\Omega_i} z d\Omega + \oint_{\partial\Omega_i} \xi \mathbf{q_{sn}} dl = 0 \tag{15}$$

where vector $\mathbf{n}$ is outward to the cell Ω_i, as displayed in Figure 1. The second integral in (14) and (15) can be explicitly expressed as a sum over the cell edges,

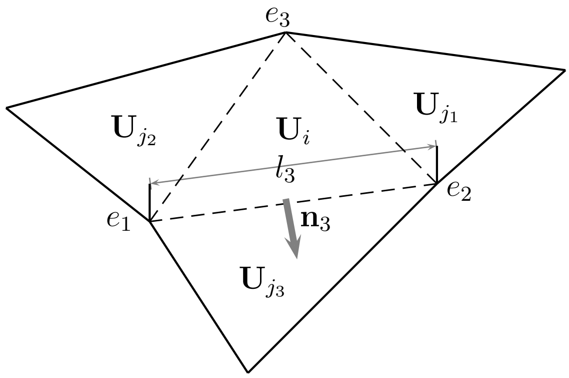

Figure 1: Cell parameters

$$\frac{\partial}{\partial t}\int_{\Omega_i}\mathbf{U}d\Omega+\sum_{k=1}^{NE}\int\mathbf{E}_{\mathbf{n}k}dl_k=\int_{\Omega}\mathbf{S}d\Omega_i \tag{16}$$

$$\frac{\partial}{\partial t}\int_{\Omega_i}zd\Omega+\sum_{k=1}^{NE}\xi\int\mathbf{q}_{\mathbf{sn}k}dl_k=0 \tag{17}$$

with $\mathbf{n}_k=(n_x,n_y)$ the outward unit vector normal to the cell edge k, dl_k is oriented with the edge and NE takes into account the number of walls which belongs to each cell i, as shown in Figure 1.

Considering a spatial discretization of first order, (16) and (17) become

$$\frac{\partial}{\partial t}\int_{\Omega_i}\mathbf{U}d\Omega+\sum_{k=1}^{NE}\mathbf{E}_{\mathbf{n}k}l_k=\int_{\Omega}\mathbf{S}d\Omega_i \tag{18}$$

$$\frac{\partial}{\partial t}\int_{\Omega_i}zd\Omega+\sum_{k=1}^{NE}\xi\mathbf{q}_{\mathbf{sn}k}l_k=0 \tag{19}$$

Also, the volume integrals of the source terms are expressed in terms of appropriate contour integrals since it is required to project the source terms on the normal direction of each cell edge,

$$\int_{\Omega_i}\mathbf{S}d\Omega_i\approx\sum_{k=1}^{NE}\int_{x'}\left[\mathbf{S}_k dx'_k\right]l_k \tag{20}$$

being x' the coordinate normal to cell edge k, as shown in Figure 2. Then, the initial system of equations in (1) is transformed in

$$\frac{\partial}{\partial t}\int_{\Omega_i}\mathbf{U}d\Omega+\sum_{k=1}^{NE}\left(\mathbf{E}_{\mathbf{n}}-\int_{x'}\mathbf{S}_k dx'\right)_k l_k=0 \tag{21}$$

System (21) and equation (19) will be solved using approximate linear solutions of initial value problems according to the Godunov method, where $\mathbf{U}_i^n$ represent the averaged value of the solution $\mathbf{U}(x,y,t)$ for each cell at time t^n

$$\mathbf{U}_i^n=\frac{1}{A_i}\int_{\Omega_i}\mathbf{U}(x,y,t^n)d\Omega \tag{22}$$

being A_i the cell area. In this way, a uniform representation of the computed variables is considered within each cell.

The development of the numerical strategy in the Godunov method is complemented by the building of an approximate solver of the Riemann problem, hereafter RP, governed by the fluxes at each side of each edge, $\mathbf{E}_j$ and $\mathbf{E}_i$ for the hydrodynamic model and $\mathbf{q_s}_j$,$\mathbf{q_s}_i$ for the morphodynamic model.

For the sake of brevity the detailed description of the two-dimensional hydrodynamic numerical scheme is omitted, since it can be found in [32, 33]. Nevertheless, the numerical method employed for computing the morphodynamic part is deeply explained in the following subsections.

3.2. Approximate Riemann Solution for the Morphodynamic model

A local 1D RP is obtained projecting the sediment fluxes onto the normal direction $\mathbf{n}_k$ of each k edge of each cell

$$\frac{\partial z}{\partial t}+\xi\frac{\partial(\mathbf{q_{sn}})}{\partial x'}=0 \tag{23}$$

Using the integral form of (23) the weak solutions associated to the RP are obtained. For this purpose an adequate control volume, Figure 3, is integrated over the following space interval $[-\Delta x', \Delta x']$, being x' sufficiently large and the time interval $[0,\Delta t]$.

$$\int_{-\Delta x'}^{+\Delta x'} z(x',t=\Delta t)\;dx'=\Delta x'\,(z_i+z_j)-\xi\delta\mathbf{q_{sn}}\Delta t \tag{24}$$

Again, the piecewise representation of the variables is hypothesized and the first order Godunov method is used for updating the averaged quantities.

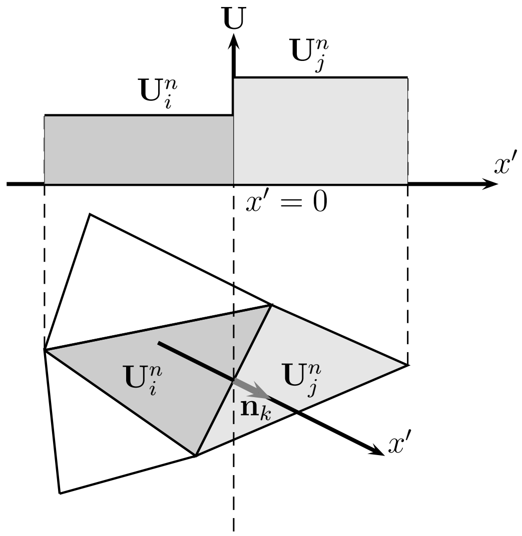

Figure 2: Riemann problem in 2D along the normal direction to a cell side

3.2.1. Consistency condition for the Morphodynamic Model

Following the philosophy employed for the hydrodynamic model in [32] a Roe approach is going to be used, i.e., the exact solution of a locally linearized problem defined by an approximate solution $\hat{z}(x,t)$ provides the solution associated to each RP. This constant linear problem is based on the definition of an approximate wave speed of the non-linear sediment flux, $\mathbf{q_{sn}}$. This following equivalent equation is written

$$\frac{\partial \hat{z}}{\partial t} + \widetilde{\lambda}_{\mathbf{bn},k} \frac{\partial \hat{z}}{\partial x'} = 0 \tag{25}$$

with the following initial conditions

$$\hat{z}(x',0) = \begin{cases} z_i & if \quad x' < 0 \\ z_j & if \quad x' > 0 \end{cases} \tag{26}$$

The approximate derived solution has to guarantee the Consistency Condition [34], forcing the fact that the integral of the exact solution (23) and the integral of the locally linearized solution, (25) to be the same. Thanks to this constraint it is derived the following expression for the wave speed which updates the bed level,

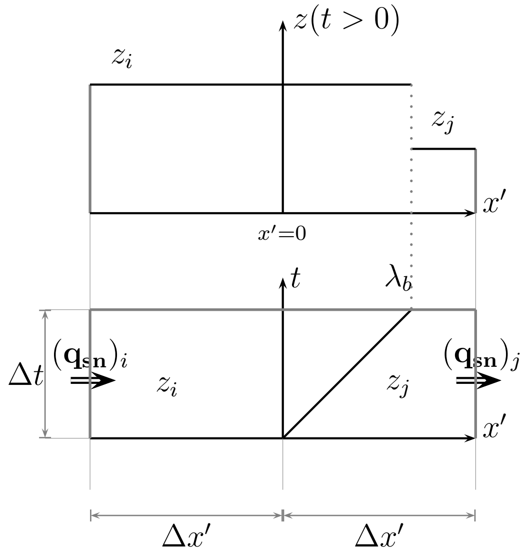

Figure 3: Suitable integral control volume

$$\widetilde{\lambda}_{\mathbf{bn},k} = \frac{\delta(\xi \mathbf{q}_{\mathbf{sn},k})}{\delta z} \tag{27}$$

with $\delta z = z_j - z_i$ and $\delta \mathbf{q}_{\mathbf{sn},k} = \mathbf{q}_{\mathbf{sn},j} - \mathbf{q}_{\mathbf{sn},i}$. Regarding equation (10) it is necessary to compute the Grass coefficient for defining the bed load discharge in each cell. Following [25] as the coefficient A_g is not a constant but varies from cell to cell, at every edge k a local $A_{g,k}$ value is defined as an arithmetic mean between neighboring cells. Consequently, the term $\delta \mathbf{q}_{\mathbf{sn},k}$ is written as $\delta \mathbf{q}_{\mathbf{sn},k} = A_{g,k} \delta \mathbf{un}_k$.

Additionally, when applying numerical modeling techniques under a flat bottom situation, the bed level difference is null and consequently the bed wave speed is not defined. In order to overcome this difficulty the computation of the friction slope, $S_{f,k}$ [32], is proposed. The friction slope is commonly used in a high number of sediment transport empirical laws, [35, 36, 37, 38], as these formulae were derived from 1D steady solid transport experiments. Additionally, its employment is coherent with the fact that transport process implies a loss of energy through the interrelationship of the flow and the particles of sediment [36, 39].

It must be stressed that the linearization of $\widetilde{\lambda}_{\mathbf{bn},k}$ in cases of almost flat bottom can lead to unphysical huge values of the bed wave speed. This is avoided by imposing a lower threshold for the bed level difference between cells: up to grain size, d_s, the approximation of the friction slope will be considered. This limitation ensures coherent values in the estimation of the bed wave speed, and wave celerity in (27) is approximated by

$$\widetilde{\lambda}_{\mathbf{bn},k} = \frac{\xi \delta \mathbf{q}_{\mathbf{sn},k}}{\delta z'} \tag{28}$$

with

$$\delta z' = \begin{cases} \delta z & if \;\; \delta z' > d_s \\ -S_{f,k} d_n & if \;\; \delta z' < d_s \end{cases} \tag{29}$$

being d_n the normal distance between cell centers, [32].

3.2.2. 2D first order finite volume for the Morphodynamic Model

The evaluation of the wave speed, $\widetilde{\lambda}_{\mathbf{bn},k}$ as in (28), brings the opportunity of splitting the sediment flux difference $\delta \mathbf{q}_{\mathbf{sn},k}$ in right-going and left-going wave propagations. Consequently the Godunov first order method is defined as

$$\delta \mathbf{q}_{\mathbf{sn},k} = \delta \mathbf{q}_{\mathbf{sn}}{}^{+}_{i,k} + \delta \mathbf{q}_{\mathbf{sn}}{}^{-}_{j,k} \tag{30}$$

with

$$\delta \mathbf{q}_{\mathbf{sn}}{}^{+}_{i,k} = \widetilde{\lambda}^{+}_{\mathbf{bn},k} \delta z_k \qquad \delta \mathbf{q}_{\mathbf{sn}}{}^{-}_{j,k} = \widetilde{\lambda}^{-}_{\mathbf{bn},k} \delta z_k \tag{31}$$

and $\widetilde{\lambda}^{\pm}_{\mathbf{bn},k} = \frac{1}{2}(\widetilde{\lambda}_{\mathbf{bn},k} \pm |\widetilde{\lambda}_{\mathbf{bn},k}|)$. Therefore,

$$z_i^{n+1} = z_i^n - \sum_{k=1}^{NE} \delta \mathbf{q}_{\mathbf{sn}}{}^{-}_{i,k} \frac{\Delta t \; l_k}{A_i} - \sum_{k=1}^{NE} \delta \mathbf{q}_{\mathbf{sn}Ii,k} \frac{\Delta t \; l_k}{A_i} \tag{32}$$

where the second term of the right side in (32) evaluates the flux in the cell edge and the third term completes the updating formula to consider the spatial variation of A_g, as it was justified in [25].

Another possibility for defining the Godunov first order method is through a flux scheme, considering outcoming and incoming fluxes through the edges of the cell. Hence the bed level is updated as

$$z_i^{n+1} = z_i^n - \sum_{k=1}^{NE} \xi \mathbf{q}^{*}_{\mathbf{sn},k} \frac{\Delta t \; l_k}{A_i} \tag{33}$$

where

$$\mathbf{q}^*_{\mathbf{sn},k} = \begin{cases} \mathbf{q}_{\mathbf{sn},i} & \text{if } \widetilde{\lambda}_{\mathbf{bn},k} > 0 \\ \mathbf{q}_{\mathbf{sn},j} & \text{if } \widetilde{\lambda}_{\mathbf{bn},k} < 0 \end{cases} \tag{34}$$

being $\mathbf{q}_{\mathbf{sn},i}$ and $\mathbf{q}_{\mathbf{sn},j}$ the bed load discharge computed in the cell i and in the cell j.

Although both numerical schemes (32) and (33) are completely equivalent, it must be stressed that the flux version is computationally more efficient, as minor algebraic operations are need. Additionally, with the flux form of the numerical scheme in (33), ghost cells must be considered in the boundary cells for completing the information required over the entire cell, [34]. The application of ghost cells almost does not penalize the computational effort. In this fashion, since the computational cost when using the flux scheme in (33) is less, this alternative has been chosen for obtaining the results displayed in the next sections.

3.3. Stability region

Updated values of $\mathbf{U}_i^{n+1}$ and z_i^{n+1} are defined after averaging the cell contributions of the local RPs, and in consequence the time step Δt has to be taken small enough so that there is no interaction of waves from the k neighboring RPs. In the 2D framework, considering unstructured meshes, the relevant distance, that will be referred to as χ_i in each cell i must consider the volume of the cell and the length of the shared k edges, [32]

$$\chi_i = \frac{A_i}{\max_{k=1,NE} l_k} \tag{35}$$

Considering that each k RP is used to deliver information to a pair of neighboring cells of different size, the distance $\min(A_i, A_j)/l_k$ is relevant, so in case that the water depth is greater than zero in all the regions of the RP solution the time step is limited by

$$\Delta t \leq CFL\, \Delta t^{\widetilde{\lambda}} \qquad \Delta t^{\widetilde{\lambda}} = \frac{\min(\chi_i, \chi_j)}{\max|\widetilde{\lambda}^m|} \tag{36}$$

with CFL=1 in case of 1D meshes, CFL=1/2 in case of 2D structured or unstructured meshes, [40] and being $\widetilde{\lambda}^m$ the water wave speeds.

When the advection structure of the problem is all contained in the system matrices, i.e. coupled-Jacobian approach [25, 19, 24], the linearised wave speeds provided by the matrices eigenvalues allow to define a suitable CFL condition, retaining the sediment transport part of the system. However, when using uncoupled/asynchronous [5] or coupled/synchronous models [8, 9, 10, 11], it has been considered traditionally that since the wave speeds associated to water surface and bed level present different magnitudes, not straightforward limitation has to be considered in the stability condition. Nevertheless, this is no longer admissible when the celerities are in the same order of magnitude. Therefore, an extra limitation linked to the bed wave speed is need

$$\Delta t \leq CFL\ \Delta t^{\widetilde{\lambda}} \qquad \Delta t^{\widetilde{\lambda}} = \frac{\min(\chi_i, \chi_j)}{|\widetilde{\lambda}^m, \widetilde{\lambda}_b|} \tag{37}$$

4. Results

This section gathers the validation tests that allow to show the assessment of the numerical schemes described in the previous sections. Numerical results have been compared with exact and experimental data considering 1D and 2D situations. The bed-load discharge law employed for computing the bed evolution, except in the exact solution test, is the Smart CFBS, which was introduced in [26]. Furthermore, in all the simulations a conservative mechanism of slope sliding failure has been considered [25] which allows to check simultaneously the bed slope and the angle of repose of saturated bed material.

4.1. Exact solution

Following [25], the first step in order to validate the numerical scheme is to test the computed solutions against exact solutions A, B and C which are summarized in Table 1. The exact solution has been built through the Riemann problems for the movable bed equations. Frictionless situations are considered and the porosity of the material is considered $p = 0.4$. The exact solutions were built by nesting several waves, departing from a left state until reaching to define the right state. The CFL condition is equal to 1.0, the mesh size is $x = 0.1m$ and the simulation is computed up to $t = 2s$. It is worth remarking that the slope sliding failure mechanism is not considered in these tests, since it could have a positive impact on the method stabilization and our wish is to verify the self-stable nature of the weakly-coupled strategy

Test	h_L	h_R	u_L	u_R	v_L	v_R	z_L	z_R
A	2.0	2.0	0.25	2.3247449	0.05	0.04	3.0	2.846848
B	2.25	1.18868612	0.20	2.4321238	0.045	0.02	5.0	5.124685
C	6.0	5.2	0.3	15.167196	0.015	0.04	3.0	4.631165

Table 1: Summary of dam break test cases with exact solution

proposed in this work. The value of the parameter A_g for the Grass law is considered as

$$A_g = \frac{A_{g,o}}{h^r} \tag{38}$$

being $A_{g,o} = 0.01$ in all cases, $r = 0$ in test cases A and B, and $r = 1$ in test case C.

In order to compare the accuracy of the weakly-coupled model (WCM) proposed in this work, the results obtained with the coupled-Jacobian technique used in [25] (CJM) are also plotted.

TestA: the solution proposed in this test case is based on two outcoming rarefaction-waves and a central shock together with a contact wave evolving downstream, Figure 4. The numerical solution is able to capture the general trend of the flow behavior, without arising numerical problems at the step area. The unit sediment discharge in both directions is also displayed.

TestB: the second solution analyzed is built through two-rarefaction waves, a contact wave and a shock, Figure 5. The computed results are able to depict the moving waves in all the wet domain with an adequate level of accuracy.

TestC: this solution is constituted by two rarefaction waves, a contact wave and a rarefaction, Figure 6. Despite of being the A_g variable, the resulting computed results follows closely the exact ones.

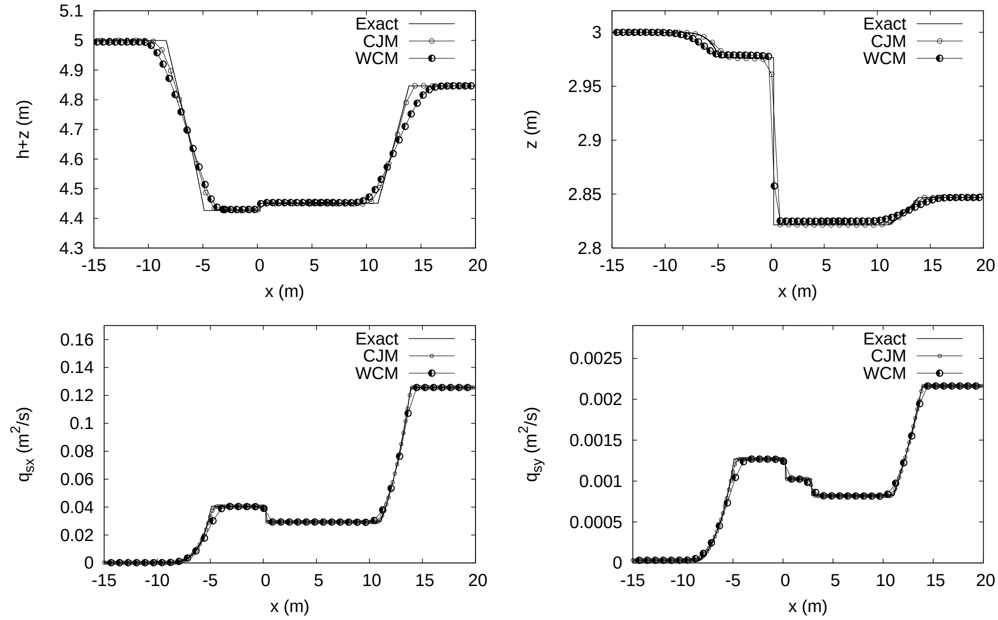

Figure 4: Exact and computed solution for Test A

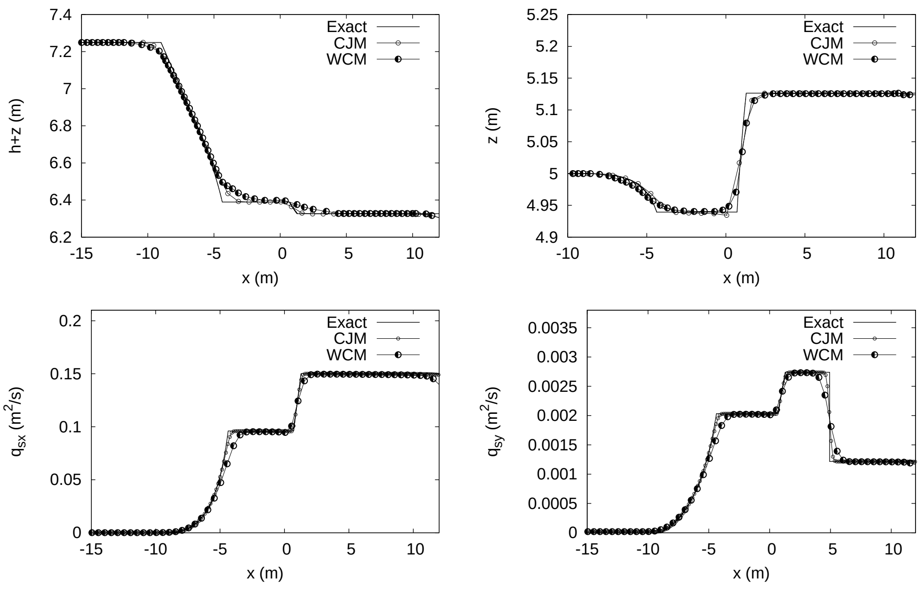

Figure 5: Exact and computed solution for Test B

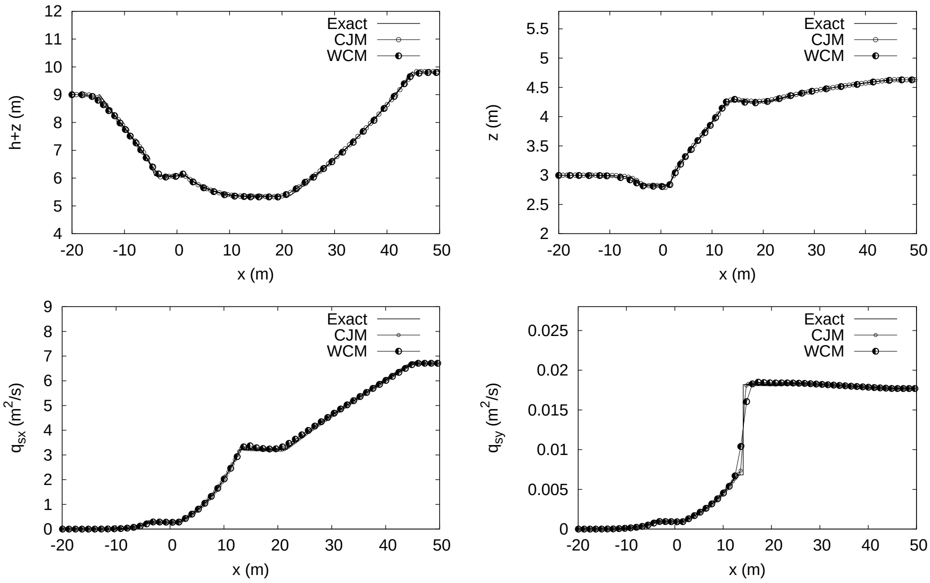

Figure 6: Exact and computed solution for Test C

4.2. 1D Dam break tests case

These experiments were performed in a channel built at the UCL Civil Engineering Department [41]. The channel had 6 m length, and in the middle a central gate was operated for simulating a dam break. The sand employed for the bed of the channel was coarse uniform sand with $d_{50} = 1.82$ mm, and the following characteristics: density $\rho_s = 2683$ kg m^{-3}, a friction angle $\varphi = 30^o$, porosity $p = 0.47$ and Manning's coefficient equal to $n = 0.0165$ sm$^{-1/3}$.

Table 2 summarizes the set of experiments selected in this work. The regions upwards and downwards the central gate were filled with different water and sand depths. Test A allows to test the numerical assessment in a situation where morphological changes are produced in presence of dry bed and a flat bottom. Test B allows checking the numerical assessment against the different type of waves that may arise in a dam break case over wet bed. Numerical simulations have been performed using $\Delta x = 0.01$ m and CFL = 1.0. No outlet condition is considered downward the channel.

Test	h_L	h_R	z_L	z_R
A	0.35	0.00	0.00	0.00
B	0.25	0.10	0.10	0.00

Table 2: Initial conditions of the test cases

4.2.1. Test A

Test A is a dam break over dry bed with an initially plane bed level. The flow evolves in time generating a left rarefaction wave upstream the gate ending in a flooding front dominated by friction. The experimental results are close to those obtained for dam break cases over dry and fixed bed [42]. Figure 7 displays numerical results and experimental data, for times ranging from 0 to 1.5 seconds. The front wave is numerically well reproduced temporally and spatially and the production of a little scour is also provided by the computed results.

As the numerical stability is one of the concerns of this work, the time step associated to the hydrodynamic and morphodynamic terms is plotted in Figure 8. Harder restriction is required by the bed movement, which justifies the inclusion of the bed wave speed in the stability condition as it has been proposed in section 3.3.

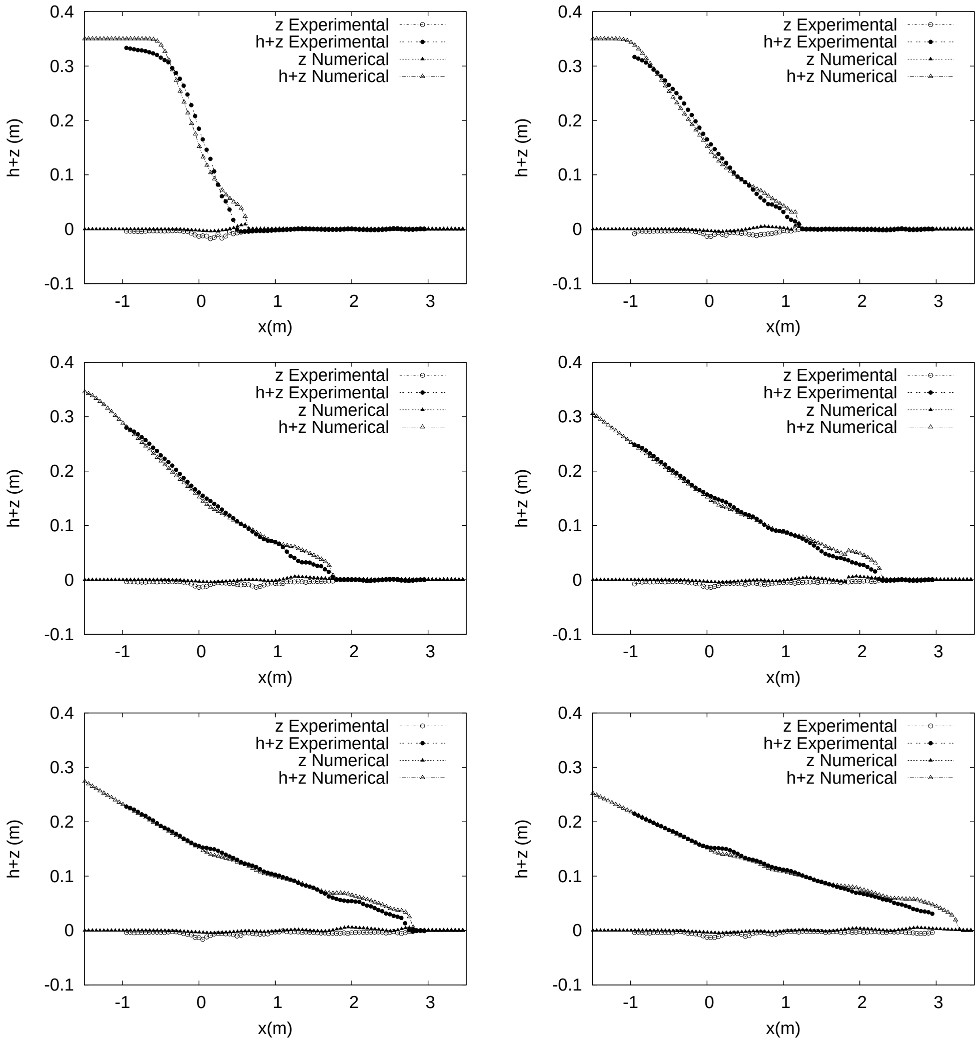

Figure 7: Numerical results and experimental data for the dam break test case A at times $t = 0.25$, 0.50, 0.75, 1.0, 1.25 and 1.5 s, using a variable value of A_g computed using Smart CFBS: measured water level surface ($-\bullet-$), measured bed level surface ($-\circ-$), computed water level surface ($-\triangle-$), measured bed level surface ($-\blacktriangle-$)

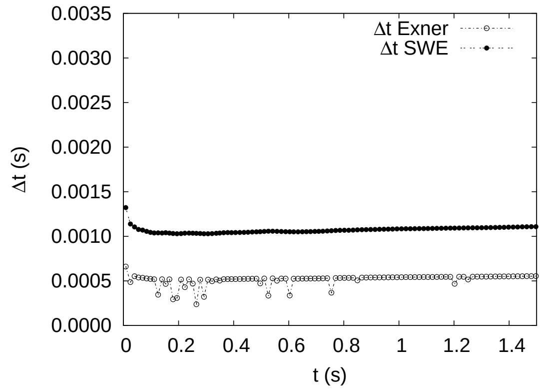

Figure 8: Time step evolution in test case A for the water waves speed as in (36), $(-\bullet-)$, and for the bed wave speed as in (37), $(-\circ-)$ during time simulation

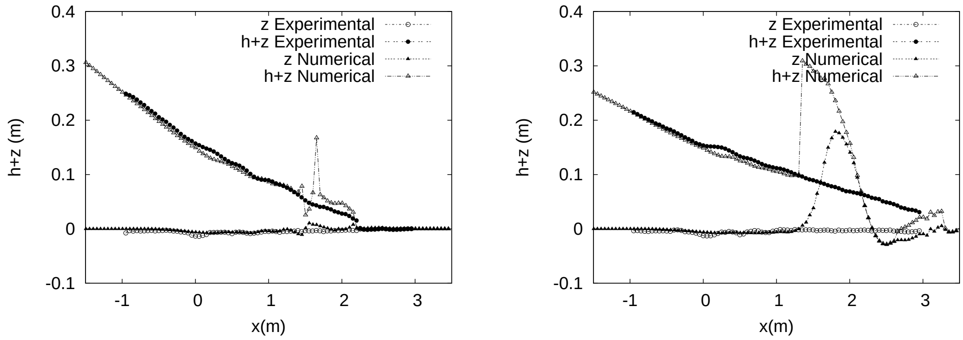

Figure 9: Numerical results and experimental data for the dam break test case A at times $t = 1.0$ and 1.5 s, when CFL limitation related to the bed speed is removed

Whether the CFL limitation related to the bed speed is removed the scheme becomes unstable as it is displayed in Figure 9 at times $t = 1.0$ and 1.5 s.

4.2.2. Test B

Test B represents the case of a bed step with a level of water downwards the gate. The flows evolves in time leading to a left moving rarefaction wave upstream the gate, followed by a steady hydraulic jump downstream the gate and finishing with a shock wave which evolves to the right side. Figure 10 gathers computed and experimental data for the free surface and bed level at different times, where it can be observed how the shock celerity is well captured by the numerical schemes. Small differences produced in the shock wave are attributable to fast transient energy variations associated to the existence of a hydraulic jump and also to the density variations of the vertical column associated to sediment concentration.

Figure 11 shows newly that the time step associated to bed wave celerity is governing the stability condition since the bed changes observed in the bottom configuration are of utmost importance.

Additionally, in Figure 12 is plotted the water level surface and the bed evolution at times t = 1.0 and 1.5 s when the CFL restriction associated to the bed wave celerity is removed. As it is expected, the scheme becomes unstable since it is not able to handle with the bed changes.

4.3. 1D Knickpoint test case

Morphological changes due to the transition between two planes with different slope (knickpoint) were measured in [43]. Thanks to this experiment is possible to compare the capacity of the numerical schemes to handle with a sudden flow transition from subcritical regime over a mild slope to supercritical regime over a steep slope. A sketch of the experiment, with the initial conditions of bed slope, is shown in Figure 13. The knickpoint is defined as the point of abrupt change in the longitudinal bottom profile of the channel.

This experiment was carried out using a coarse and uniform size sand with the following properties $\rho_s = 2680 kgm^{-3}$, $d_{50} = 1.65mm$, $\varphi = 30^o$, negligible cohesion, porosity $p = 0.42$ and a Manning's coeffcient, $n = 0.0165$ sm$^{-1/3}$. Initial conditions employed are: upstream, water level surface (0.028 m) and discharge (9.8 l/s); downstream, a known water surface level at the end of the flume (0.11 m). The domain, 7.4 meters long, is divided using Δx = 0.05 m. In all simulations CFL = 1.

Bed level variation in the longitudinal profile was recorded in time and is compared with the predictions supplied by the numerical schemes in Figure 14. The computed solution describes a good trend when comparing with the experimental solution. The erosion located in the knickpoint is predicted at the same rate as the experiment and the final bottom is also well achieved.

Since in this experimental case an important change in the bottom morphology takes place, Figure 15 shows the more restrictive time step associated to the wave speeds of water and bed in time simulation. Bed time step imposes a harder restriction than the fluid flow and for this reason has to be considered in (36) for preserving the numerical stability of the numerical scheme.

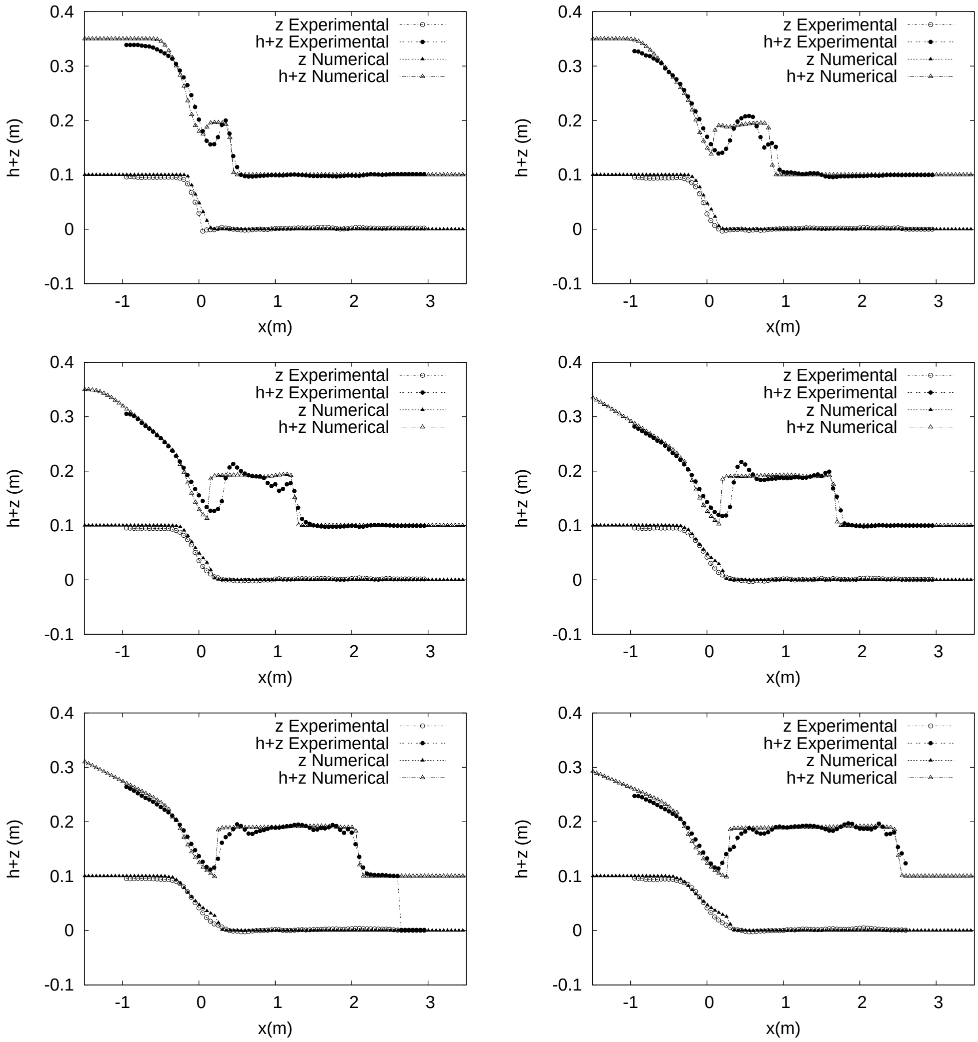

Figure 10: Numerical results and experimental data for the dam break test case B at times $t = 0.25$, 0.50, 0.75, 1.0, 1.25 and 1.5 s, using a variable value of A_g computed using Smart CFBS: measured water level surface ($- \bullet -$), measured bed level surface ($- \circ -$), computed water level surface ($-\triangle-$), measured bed level surface ($-\blacktriangle-$)

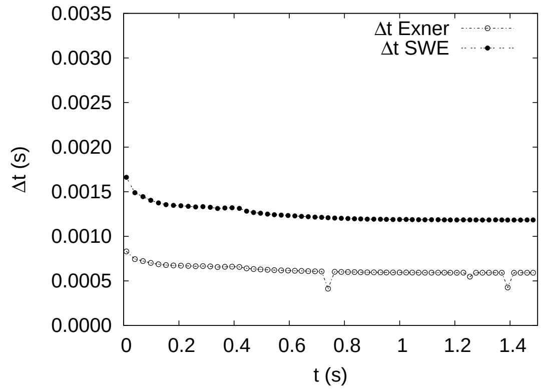

Figure 11: Time step evolution in test case B for the water waves speed as in (36), $(-\bullet-)$, and for the bed wave speed as in (37), $(-\circ-)$ during time simulation

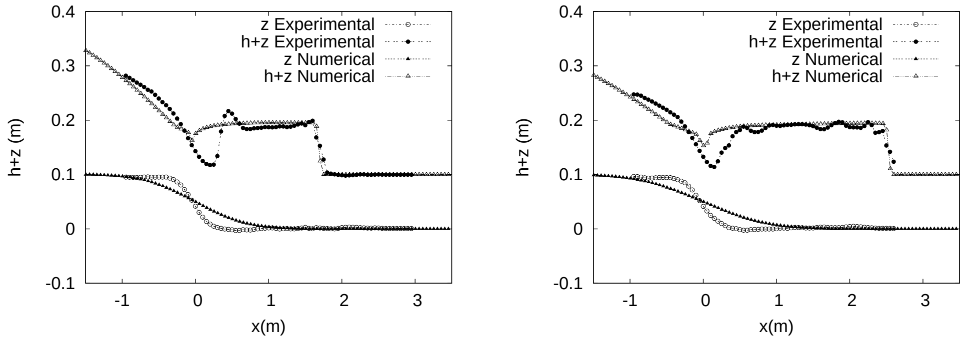

Figure 12: Numerical results and experimental data for the dam break test case B at times $t = 1.0$ and 1.5 s, when CFL limitation related to the bed speed is removed

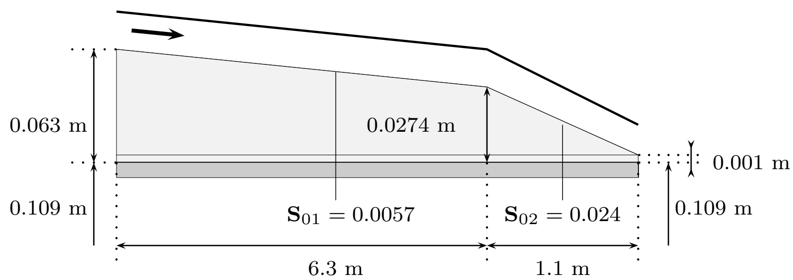

Figure 13: Knickpoint sketch

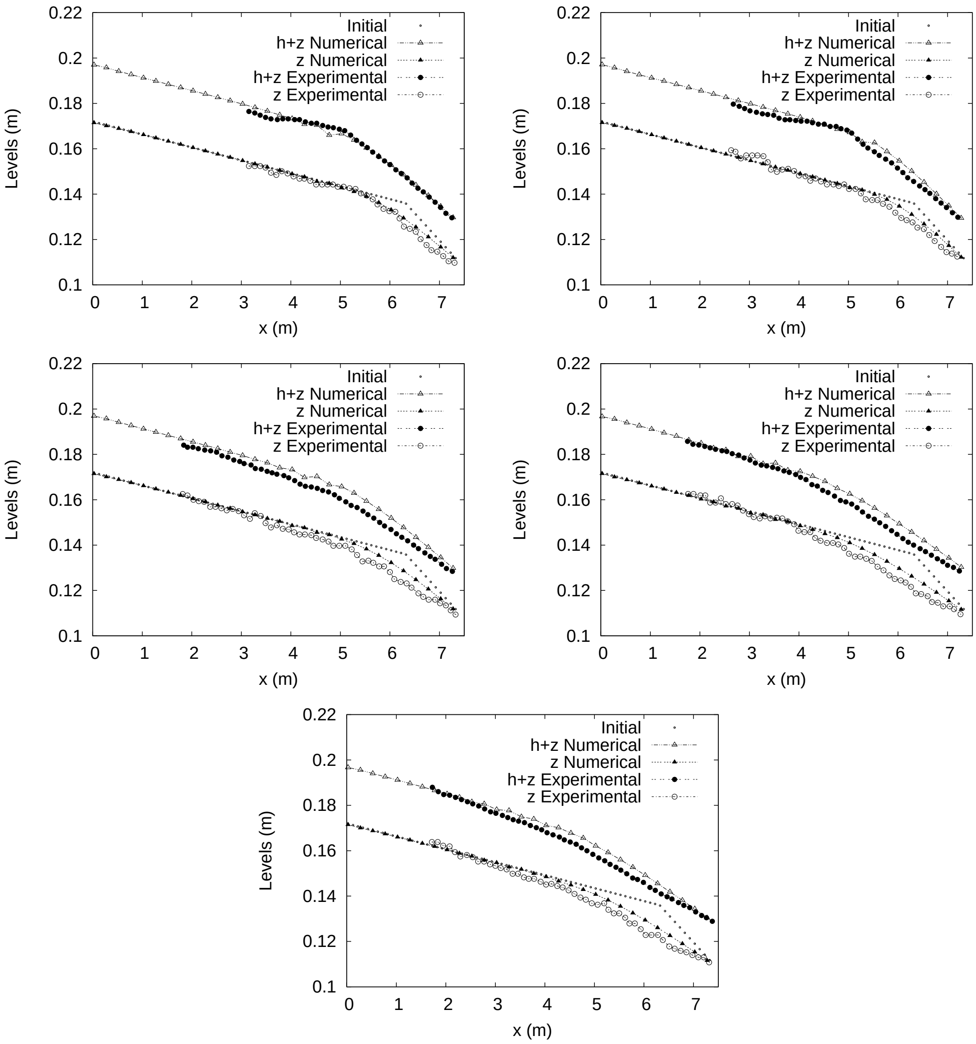

Figure 14: Results for the knickpoint test case. Initial bed level $(\cdots)$, measured bed and water level $(-\bullet-)$ and computed $(-\triangle-)$ at times t = 165, 223, 345, 589 and 851 s with variable value of A_g computed using Smart CFBS

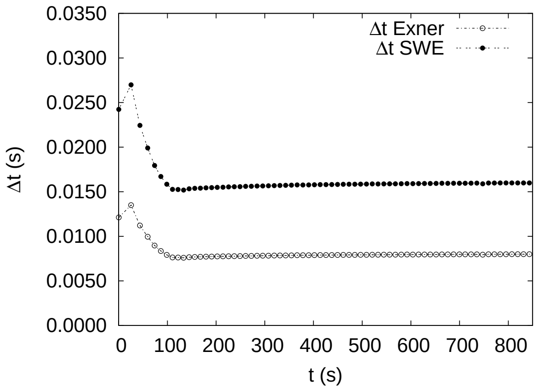

Figure 15: Time step evolution for the water waves speed, as in (36), $(-\bullet-)$, and for the bed wave speed as in (37), $(-\circ-)$ during time simulation

4.4. 2D Numerical modeling of dam failure

Another important problem related to erosion process is the dam failure by overtopping. This feature was studied by Tingsanchali et al. in [44]. In this problem the inclusion of the slope failure model is quite relevant. The laboratory setup employed during the experiment is displayed in Figure 16. In the present work the laboratory data from case B1 is employed for validating the computational predictions. It must be stressed that being the flow mostly one-dimensional, it is important to check the numerical performance of the solution in a 2D mesh to ensure that it is not governed by the mesh topology. This case is of great interest, as it allows a direct comparison in a wide variety of flow conditions.

Following prior work developed in [26] the 2D numerical simulation has been performed using a coarse unstructured triangular mesh, with a maximum cell size of 0.01m^2. The mesh together with the initial water depth is displayed in Figure 17. CFL is imposed equal to 0.5. Free boundary condition is considered at the outflow section. Figure 18 displays the bed level evolution when using Smart CFBS formulation. At the crest of the dike strong erosion occurred because of the strong initial discontinuity of water depth and the severe slope downwards the gate. The granular material of the dike is completely mobilized rapidly in time and it is grabbed downstream the dam by the flow.

Figure 19(a) shows the bed and water surface calculated after 120 s when using Smart CFBS formulation. As the bed level was temporally measured

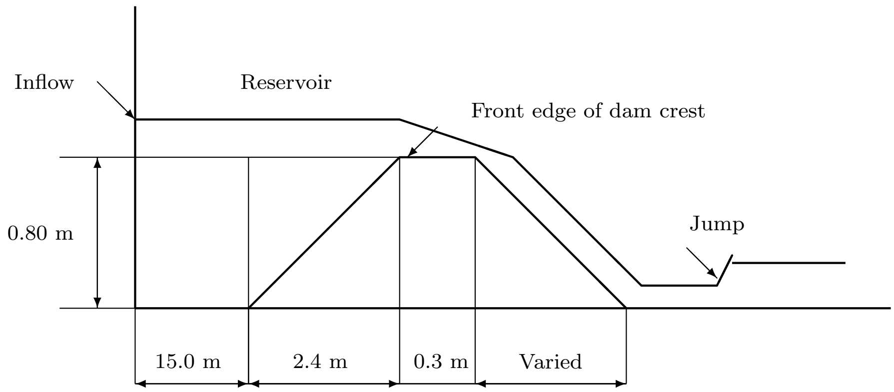

Figure 16: Sketch of the dam failure experimental setup

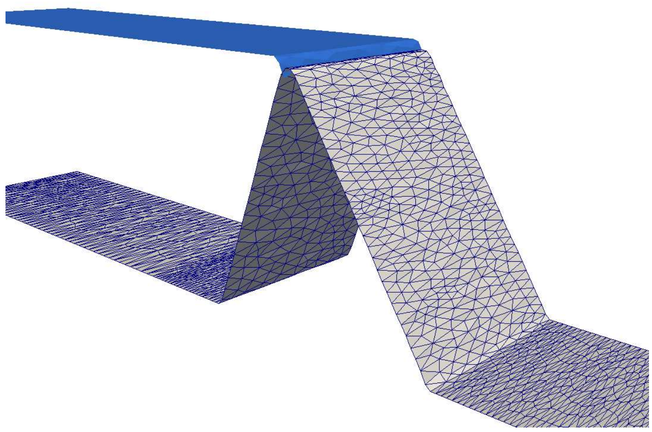

Figure 17: Detail of the triangular mesh and initial condition for the water depth

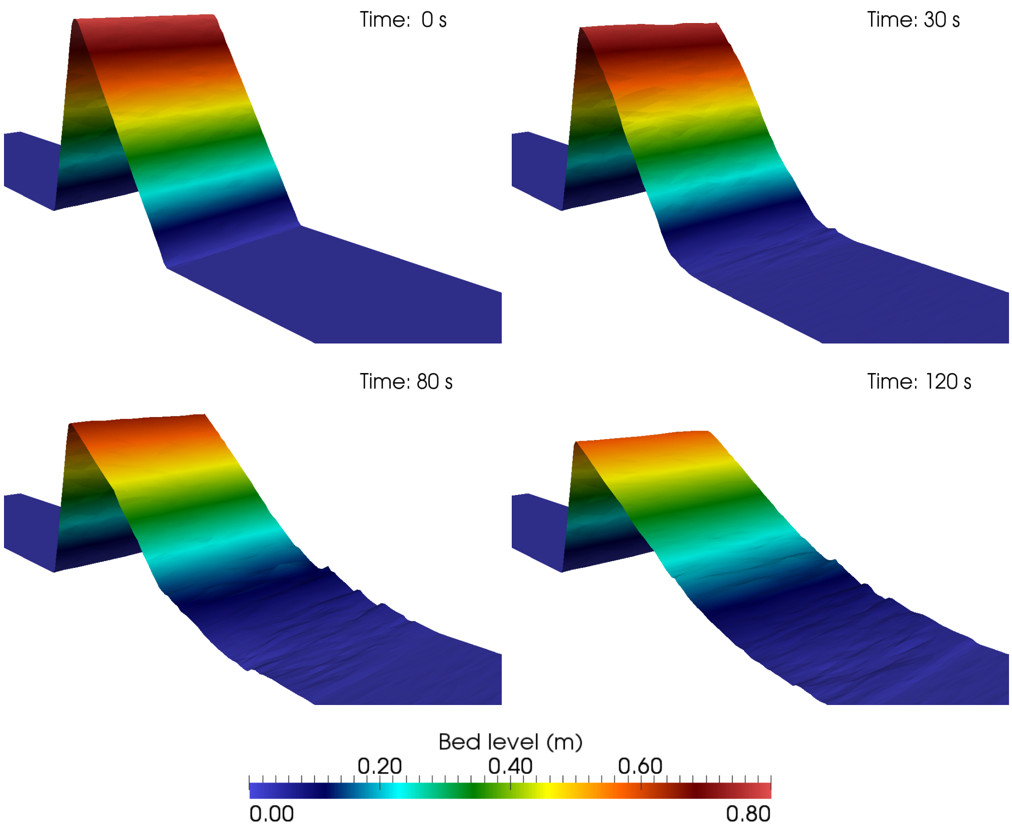

Figure 18: Computed results of the bed level evolution when using a variable value of A_g built with Smart CFBS and at times t = 0, 30, 80 and 120 s

at three points SA, SB and SC, placed downwards the dam, the comparison between experimental data and computed results are displayed in Figure 19(b). Numerical results are able to handle the strong morphodynamics changes which take place without displaying numerical oscillations and additionally, well tracking the experimental data. On the other hand, the experimental and computed water reservoir surface level is displayed in Figure 19(c). Figure 19(d) depicts the overtopping discharge obtained numerically and experimentally. Both measurements provide high quality and useful information about this type of phenomena. Numerical schemes allows to obtain a good detail of forecasting capacity for the bed and water level evolution together with an efficient computational cost.

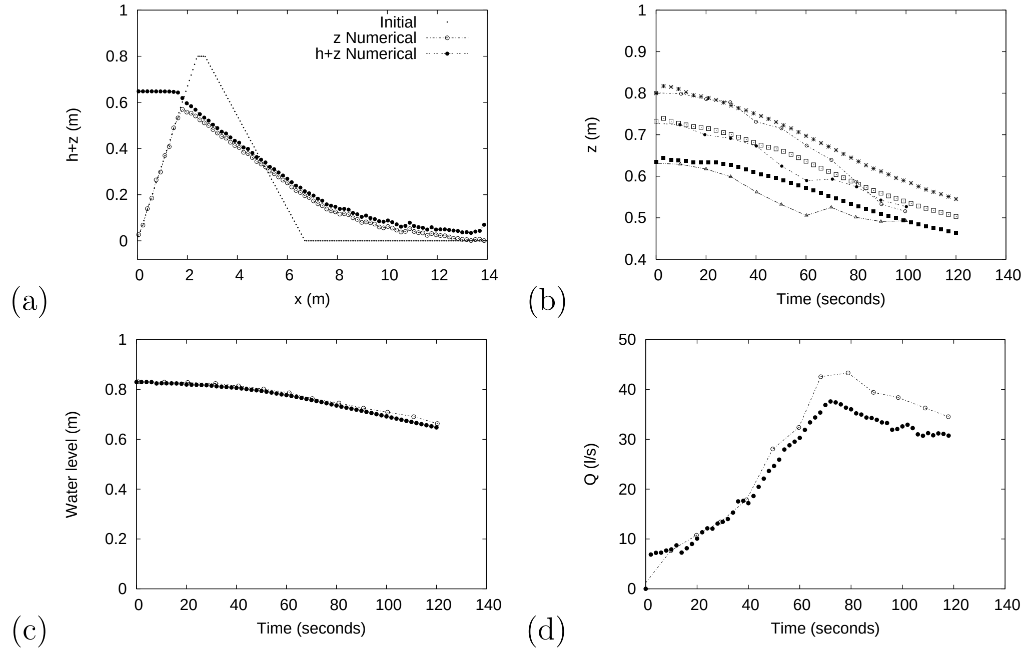

Figure 19: (a) Initial bed level (- - -), computed water level surface (−△−) and bed level surface (−▲−) at $t = 120$ s. (b) Bed level surface evolution in time measured at stations SA (− ○ −) (−□−), SB (− ● −), and SC (−△−) and computed at stations SA (− ⋆ −),SB (−□−), and SC (−■−). (c) Evolution in time of the measured water reservoir level (− ○ −) and computed water reservoir level (− ● −). (d) Evolution in time of the measured (− ○ −) and computed (− ● −) overtopping discharge

For this test case, the time step evolution associated to each wave speed is also studied, Figure 20. Initially, heavier restrictions are required by the water flow, as the overtopping event has not provoked yet the dike failure. However, as time advances and the geomorphic changes become more severe, time step restrictions come from the bed celerity. At the end of time simulation, where most of the sediment particle movement has occurred, the time step is newly governed by flow characteristics. In view of these results, it is proved the efficiency of the solver, as only when important bed changes exist the classical time step of water flow is decreased.

Additionally to the study of the time step evolution this test case has been chosen also for comparing the computational time cost with respect to the coupled-Jacobian technique used in [25] (CJM) and the weakly-coupled model (WCM) proposed in this work. For this purpose three meshes with

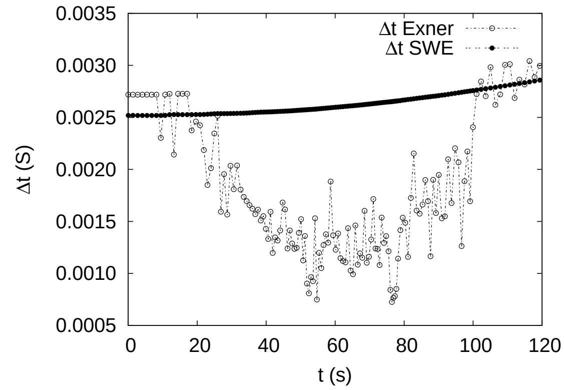

Figure 20: Time step evolution for the water waves speed, as in (36), $(-\bullet-)$, and for the bed wave speed, as in (37), $(-\circ-)$ during time simulation

increasing number of elements are considered. In Table 3 are displayed the ratio between the computational cost when employing [25] and when considering the procedure explained in this work. Results plotted above belongs to the second mesh. Noticeable computational efficiency is achieved, being more important as the level of mesh refinement is increased. The computational cost time with the CJM is penalized by the high number of algebraic operations need for computing the eigenvalues and eigenvectors. In order to support this fact and employing the second mesh, the time step evolution, associated to the CJM and to WCM is displayed in Figure 21. Despite of presenting a bigger time step on average when using the CJM, the computational cost is higher.

N. of elements	*Ratio of computational cost time* $= CJM/WCM$
2000	8.46
4100	10.15
8300	13.72

Table 3: Summary of ratios of computational cost time when using the JCM technique and the WCM technique

Together with the computational cost time, the RMSE (Root median square error) for the three stations SA, SB and SC obtained when using the coupled-Jacobian model from [25] (CJM) and the weakly-coupled model (WCM) proposed in this work, is displayed in Table 4. The weakly-coupled model provides computational results close to the experimental ones whilst

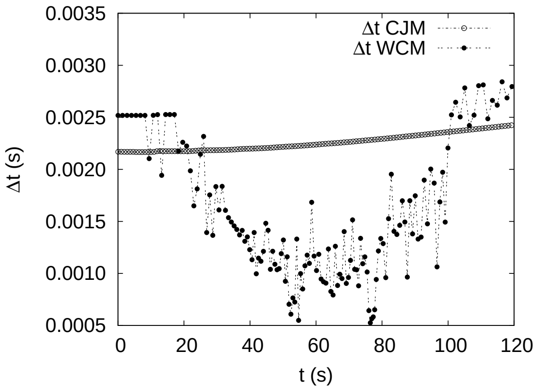

Figure 21: Time step evolution following the CJM technique in [25], $(- \circ -)$, and the WCM technique explained in this work, $(- \bullet -)$ during time simulation

the computational time is decreased.

N. of elements	$RMSE(m)$ SA		$RMSE(m)$ SB		$RMSE(m)$ SC	
	CJM	WCM	CJM	WCM	CJM	WCM
2000	0.065	0.039	0.042	0.034	0.058	0.037
4100	0.043	0.021	0.028	0.019	0.038	0.023
8300	0.028	0.014	0.019	0.012	0.025	0.015

Table 4: Summary of the RMSE associated to each station when using the JCM technique and the WCM technique

4.5. 2D Dam break with an abrupt expansion

This experiment was numerically reproduced in [26] with a coupled model. It consist of a dam break over a dry and erodible bed experiment. It was performed at the laboratory of the Civil and Environmental Engineering Department of the UCL [45, 46]. The laboratory set up employed in the experiment is shown in Figure 22. The sediment was uniform sand with the following properties: median diameter $d_{50} = 1.65$ mm, density $\rho_s = 2630$ kg m^{-3}, friction angle $\varphi = 15^o$, negligible cohesion, porosity $p = 0.42$ and Manning's factor equal to $n = 0.0185$ sm$^{-1/3}$. During the development of the experiment the water fluctuation was measured at different points as well as the final bed surface at several cross sections, Figure 23 and Tables 5, 6. An unstructured mesh is considered and CFL condition is imposed equal to 0.5.

This experimental case represents a complete challenge as it gathers several highlighted situations which can occur in the real engineering life: an

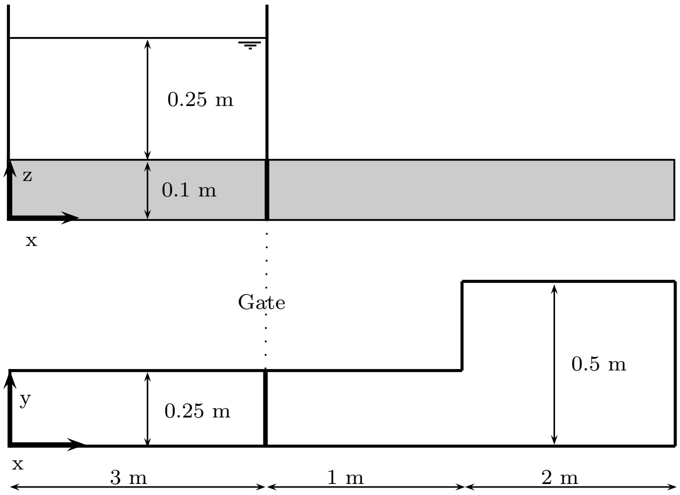

Figure 22: Sketch of the experimental flume: side view (upper) and plan view (lower)

Figure 23: Plan view of the experimental flume. Locations of the probes (left) and the cross sections (right)

Probe	$Xcoordinate(m)$	$Ycoordinate(m)$
U1	3.75	0.125
U2	4.20	0.125
U3	4.20	0.375
U4	4.45	0.125
U5	4.45	0.375
U6	4.95	0.125
U7	4.95	0.375

Table 5: Position of the probes

area where the flow is genuinely one-dimensional, an abrupt expansion which provokes the change to a two-dimensional flow, important velocity gradients which create a recirculating area, moving shocks close to the wall zone and moreover a severe local erosion together with a noticeable sediment deposition area. It constitutes the perfect benchmark for checking the assessment

Section	$X coordinate (m)$
S1	4.10
S2	4.20
S3	4.30
S4	4.40
S5	4.50

Table 6: Position of the sections

of the numerical schemes against sudden and strong changes in the flow and the bed. Due to these characteristics other authors have also studied recently this test case [21, 11, 24].

This experimental test is very sensitive to bed deformation since the flow evolves over an initially dry bed: sediment particles start to bounce as soon as the water reaches their position. As it was observed in the work of [45, 46] once the water overtakes the corner of the channel the flow expands, causing the water depth to decrease and the bed level suffers a dramatic local erosion. Close to the wall area the flow tends to slow down and the material grabbed upstream is settled. In this zone of the channel the loss of energy is so strong that a bed sharp surface emerges. Downstream, the sediment grains are pushed outward the domain and eventually intersects driving to settling zones. At the last time, the drainage of water leads to soften the bed surface although the minimum and maximum sediment peak areas are clearly identified.

Once the experiment has been qualitatively described, computed and experimental data are faced. Comparison between the water level measured and the numerical solution is showed in Figure 24. The majority of the probes achieve a good trend in relation with the experimental data. Probes U3 and U4 are the ones which provide less accurate results. This is justified by the fact that they are located close to the expansion (probe U3) and close to the wall (probe U4), where three dimensional flow structures are generated due to the sudden expansion and the shock against the lateral side. With the present mathematical model, where the set of equations is depth-averaged, the vertical accelerations are neglected and consequently, this flow behavior cannot be properly treated [11].

Figure 25 gathers the measured bed level after the dam break event and the numerical predictions at control sections S1, S2, S3, S4 and S5. In all the sections the computed bed surface is able to follow the measured evolution. Section S1 which is the closest to the expansion does not obtain neither the maximum nor the minimum of sediment peaks, although the prediction follows the sediment movement pattern: particles are grabbed from left and settled to the right bank. In control sections, S2, S3 and S4, the computed bed surface follows correctly the tendency of the final bed morphology although the final bed slopes are less sharp than the ones recorded after the experiment. As it has been noted before, since the mathematical model is depth-averaged the vertical accelerations are not considered. Consequently, the erosion/deposition rates are decreased and differences in the granular material lying close to the right wall are expected. Section S5, positioned far away from the area of stronger influence, obtains a good tendency when comparing with the experimental data.

Comparison of the computational cost time and the accuracy obtained when using the coupled-Jacobian model (CJM) from [25] and the weakly-coupled model (WCM) proposed in this work is displayed in Table 7. For the sake of brevity only the RMSE associated to section S2 is showed. The CJM technique provides more accurate results in this case at the cost of increasing the computational time.

$N.\ of\ elements$	$Ratio\ of\ computational\ cost\ time : CJM/WCM$	$RMSE(m) : S2$	
		CJM	WCM
2000	5.23	0.015	0.024
4300	8.15	0.009	0.015
8100	14.02	0.006	0.012

Table 7: Summary of ratios of computational cost time and the RMSE for section S2 when using the CJM technique and the WCM technique

5. Conclusions

A 2D numerical scheme for wave flows over mobile beds has been detailed. The numerical scheme solves a weak coupled model which includes the 2D SWE and the 2D Exner sediment continuity equation. It is written considering a finite volume method based on a Roe type solver and allows to verify that stable results can be obtained without employing coupled-Jacobian and computationally expensive scheme. Following prior works the generalization for several solid discharge laws has been taken into account. The explicit scheme has shown dynamic stability, always controlled by an augmented CFL condition.

The first two experimental cases considered, developed in 1D, have been performed to solve dam break situations over dry/wet initial conditions and with different morphodynamic configuration. Advance front celerity has been well captured in the dam break as well as the bed changes. Regarding the 1D knickpoint test case, the existence of variable flow regime or morphodynamic discontinuities does not ruin the forecast capacity of the numerical scheme leading to stable results.

Regarding the bidimensional cases, the comparison with the exact solutions showed that the computed results are similar to the ones obtained with a coupled-Jacobian model. In the next experiment, the dike collapse by overtopping, numerical performance of the solution in a 2D mesh is checked under severe changes in the bed surface level. Self-stable results have been obtained for both the water level and the bottom changes. Finally, in the 2D dam break with an abrupt expansion numerically reproduced, the free surface and bed level predictions have been well computed in time and space.

Since in practical applications, both stability and efficiency characteristics are required, the main challenge of this work has been to combine the interactions between flow and bed without using a coupled-Jacobian matrix as the proposed in [25] with a higher computational effort. Also, when plotting the time step restrictions associated to the water wave celerities and to the bed wave celerity it has been checked how only severe changes in bottom morphology affect the time step restriction of the weakly-coupled model proposed in this work.

Lastly, regarding the point of efficiency and as a future research, the proposed explicit finite-volume Godunov-type numerical scheme should be compared in terms of efficiency and accuracy with other implicit numerical techniques suggested in the literature [31, 47]. When employing an implicit strategy the time step chosen can be bigger in relation with an explicit however, the main drawback is the convergence speed of the linear solver employed for computing the solution of the algebraic system. A throughly study should be addressed.

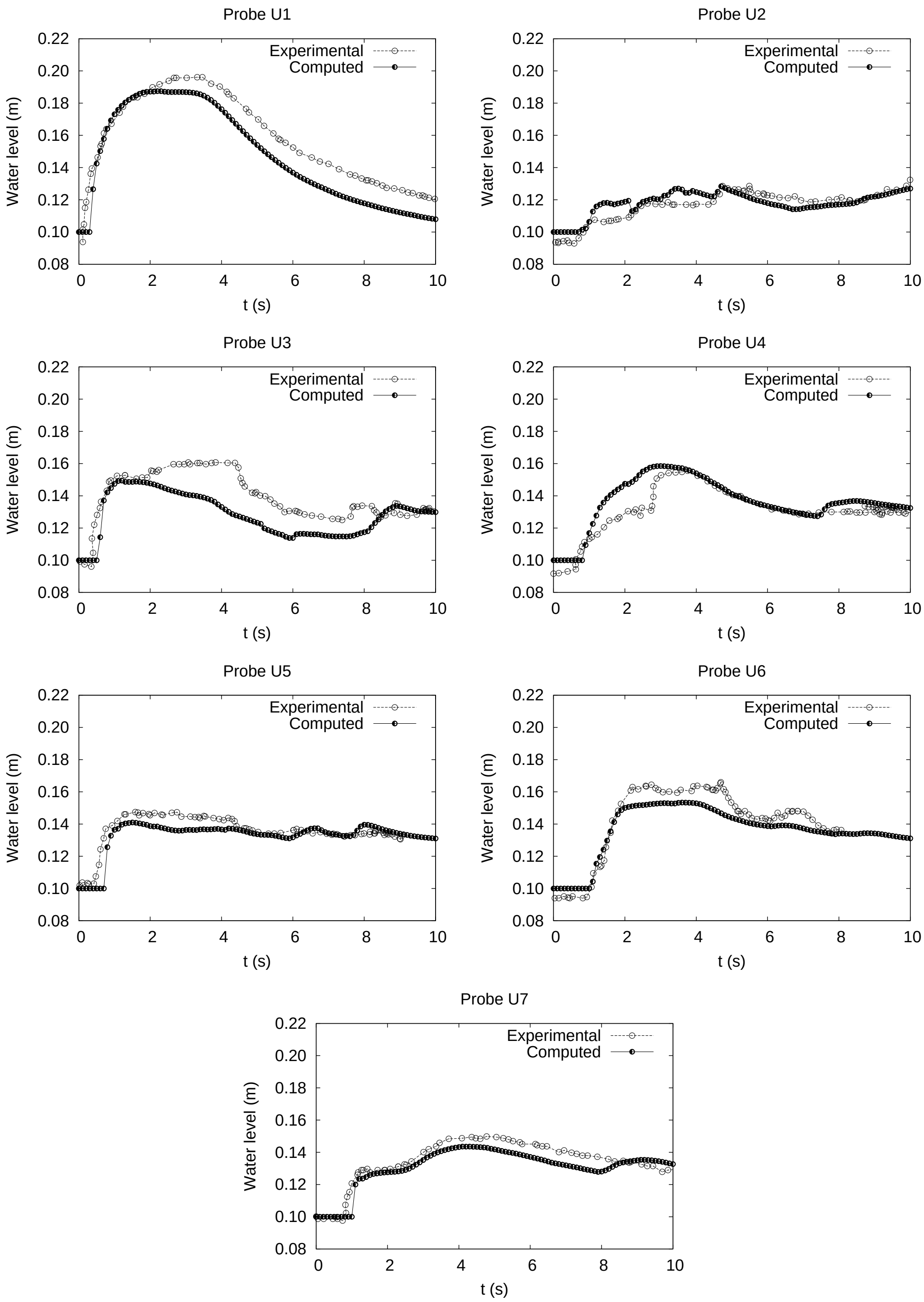

Figure 24: Temporal comparison between experimental ($-\circ-$) and computed ($-\bullet-$) results for the water level at probes U1-U7

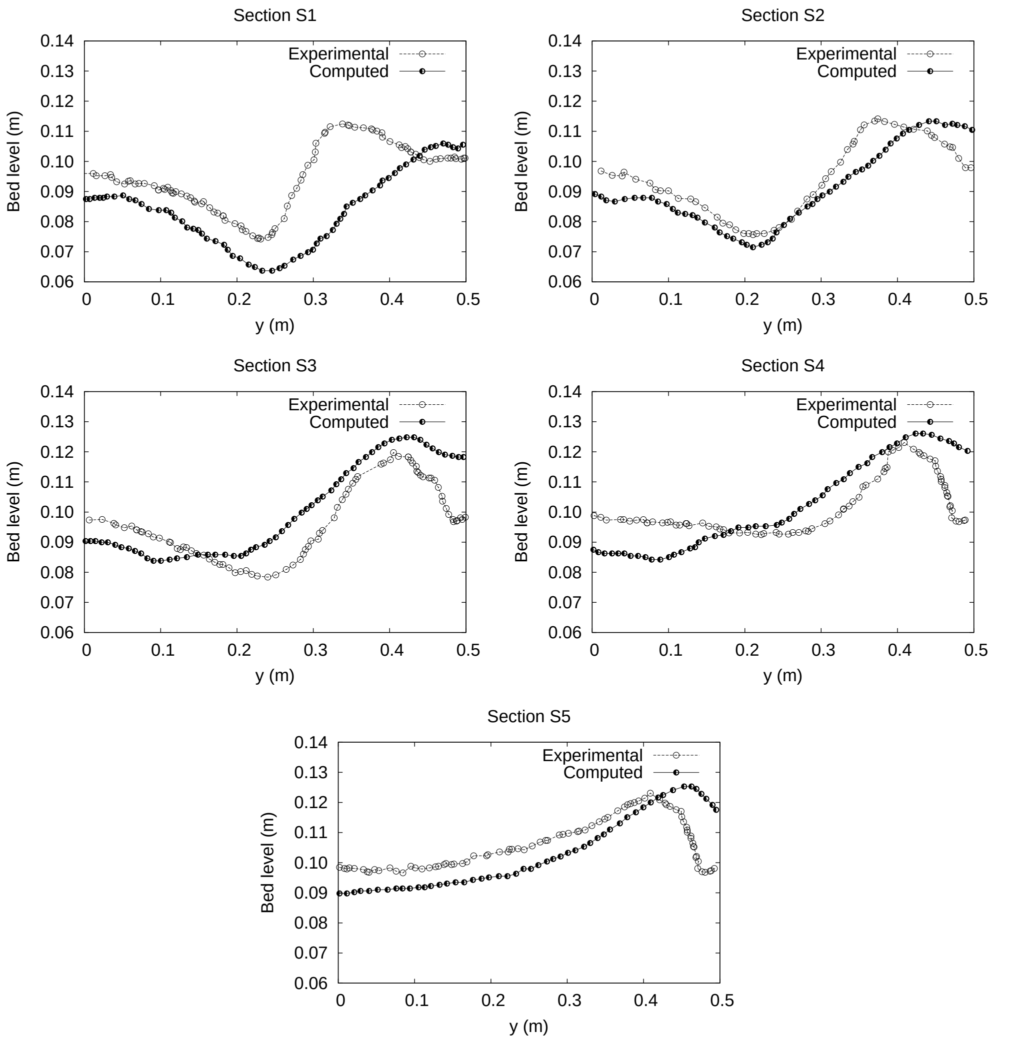

Figure 25: Comparison of the experimental ($-\circ-$) and computed ($-\bullet-$) final bed surface at cross sections S1-S5

References

[1] Nielsen P. Coastal Bottom Boundary Layers and Sediment Transport. Advanced Series on Ocean Engineering. World Scientific Publishing; 1992.

[2] Julien P. Erosion and Sedimentation. Cambridge University Press; 1998.

[3] Hudson J, Sweby PK. Formulations for Numerically Approximating Hyperbolic Systems Governing Sediment Transport. Journal of Scientific Computing 2002;19:225–251. doi:10.1023/A:1025304008907.

[4] Hudson J, Sweby PK. A high-resolution scheme for the equations governing 2D bed-load sediment transport. Int J Numer Meth Fluids 2005;47:1085–1091. doi:10.1002/fld.853.

[5] De Vriend H, Zyserman J, Nicholson J, Roelvink J, Pechon P, Southgate H. Medium-term 2DH coastal area modelling. J Coastal Eng 1993;21:193–224.

[6] Abderrezzak KK, Paquier A. Applicability of Sediment Transport Capacity Formulas to Dam-Break Flows over Movable Beds. J Hydraul Eng 2011;137:209–221. doi:10.1061/(ASCE)HY.1943-7900.0000298.

[7] Aricò C, Tucciarelli T. Diffusive Modeling of Aggradation and Degradation in Artificial Channels. J Hydraul Eng 2008;134(8):1079–1088. doi:10.1061/(ASCE)0733-9429(2008)134:8(1079).

[8] Holly FM, Rahuel JL. New numerical/physical framework for mobile-bed modelling. I: Numerical and physical principles. J Hydraul Res 1990;28(4):401–416.

[9] Cao Z, Day R, Egashira S. Coupled and decoupled numerical modeling of flow and morphological evolution in alluvial rivers. J Hydraul Eng 2002;128:306–321.

[10] Wu W, Wang S. Depth averaged two dimensional numerical modelling of unsteady flow and non uniform sediment transport in open channels. J Hydraul Eng 2004;130:1013–1024.

[11] Xia J, Lin B, Falconer R, Wang G. Modelling Dam-break Flows over Mobile Beds using a 2D Coupled Approach. Adv Water Res 2010;33:171–183. doi:10.1016/j.advwatres.2009.11.004.

[12] Cordier S, Le M, Morales de Luna T. Bedload transport in shallow water models: Why splitting (may) fail, how hyperbolicity (can) help. Adv Water Res 2011;34:980–989. doi:10.1016/j.advwatres.2011.05.002.

[13] Wu W, Marsooli R, He Z. Depth-Averaged Two-Dimensional Model of Unsteady Flow and Sediment Transport due to Noncohesive Embankment Break/Breaching. J Hydraul Eng 2012;138(6):503–516. doi:10.1061/(ASCE)HY.1943-7900.0000546.

[14] Kassem AA, Chaudry MH. Comparison of coupled and semicoupled numerical models for alluvial channels. J Hydraul Eng 1998;124(8):794–802.

[15] Tassi P, Rheberg S, Vionnet C, Bokhove O. Discontinous Galerkin finite element for river bed evolution under shallow flows. Com Meth App Mech Eng 2008;197:2930–2947.

[16] Cao Z, Pender G, Carling P. Shallow water hydrodynamic models for hyperconcentrated sediment-laden flows over erodible bed. Adv Water Res 2006;29(4):546–557.

[17] Lyn D, Altinakar M. St. Venant-Exner equations for near-critical and transcritical flows. J Hydraul Eng 2002;579:579–587. doi:10.1061/(ASCE)0733-9429(2002)128:6(579).

[18] Grass A. Sediments transport by waves and currents. SERC London Cent. Mar. Technol, Report No. FL; 1981.

[19] Castro Diaz M, Fernandez Nieto E, Ferreiro A, Parés C. Two-dimensional sediment transport models in shallow water equations. A second order finite volume approach on unstructured meshes. Computer Methods in Applied Mechanics and Engineering 2009;198:2520–2538. doi:10.1016/j.cma.2009.03.001.

[20] G. Dal Maso P.G. LeFloch FM. Definition and weak stability of non-conservative products. Math Pures Appl 1995;74:483–548.

[21] Soares-Frazao S, Zech Y. HLLC scheme with novel wave-speed estimators appropiate for two-dimensional shallow-water flow on erodible bed. Int J Numer Meth Fluids 2010;66(8):1019–1036. doi:10.1080/00221686.2012.689682.

[22] Rosatti G, Murillo J, Fraccarollo L. Generalized Roe schemes for 1D, two-phase, free-surface flows over a mobile bed. J Comput Phys 2008;227(4):10058–10077.

[23] Canestrelli A, Dumbser M, Siviglia A, Toro E. Well-balanced high-order centred schemes on unstructured meshes for shallow water equations with fixed and mobile bed. Adv Water Res 2010;33:291–303. doi:10.1016/j.advwatres.2009.12.006.

[24] Siviglia A, Stecca G, Vanzo D, Zolezzi G, Toro E, Tubino M. Numerical modelling of two-dimensional morphodynamics with applications to river bars and bifurcations. Adv Water Res 2013;52:243–260. doi:dx.doi.org/10.1016/j.advwatres.2012.11.010.

[25] Murillo J, García-Navarro P. An Exner-based coupled model for two-dimensional transient flow over erodible bed. J Comput Phys 2010;229:8704–8732. doi:10.1016/j.jcp.2010.08.006.

[26] Juez C, Murillo J, García-Navarro P. Numerical assesment of bed load discharge formulations for transient flow in 1D and 2D situations. J Hydroinform 2013;-:In press. doi:10.2166/hydro.2013.153.

[27] Serrano A, Murillo J, García-Navarro P. Finite volumes for 2D shallow-water flow with bed-load transport on unstructured grids. J Hydraul Res 2012;50(2):154–163. doi:10.1080/00221686.2012.669142.

[28] Akanbi A, Katopodes N. Model for flood propagation on initially dry land. J Hydraul Eng 1987;114:689–706.

[29] Kalinske A. Movement of sediment as bed load in rivers. Trans AGU 1947;28:615–620.

[30] De Vries M, Klaassen G, Struiksma N. On the use of movable-bed models for river problems: a state of the art. Int Journ of Sediment Research 1990;5(1):35–47.

[31] Garegnani G, Rosatti G, Bonaventura L. On the range of validity of the Exner-based models for mobile-bed river flow simulations. J Hydraul Res 2013;51(4):380–391. doi:10.1080/00221686.2013.791647.

[32] Murillo J, García-Navarro P. Weak solutions for partial differential equations with source terms: Application to the shallow water equations. J Comput Phys 2010;229:4327–4368. doi:10.1016/j.jcp.2010.02.016.

[33] Murillo J, García-Navarro P. Wave Riemann description of friction terms in unsteady shallow flows: Application to water and mud/debris floods. J Comput Phys 2012;231:1963–2001. doi:10.1016/j.jcp.2011.11.014.

[34] Leveque R. Finite Volume Methods for Hyperbolic Problems. Cambridge University Press, New York; 2002.

[35] Meyer-Peter E, Müller R. In: Report on the 2nd Meeting International Association Hydraulic Structure Research. Stockholm, Sweden; 1948.

[36] Smart G. Sediment transport formula for steep channels. J Hydraul Eng 1984;3:267–276.

[37] Ashida K, Michiue M. Study on hydraulic resistance and bedload transport rate in alluvial streams. Transactions, Japan Soc Civil Eng 1972;206:569–589.

[38] Camenen B, Larson M. A general formula for non-cohesive bed load sediment transport. Estuarine, Coastal and Shelf Science 2005;63:249–260.

[39] Whittaker J, Davies T. Erosion and sediment transport processes in step-pool torrents. Hydrological Sciences Journal-Journal des Sciences Hydrologiques 1982;27(2):234–244.

[40] Toro E. Riemann solvers and numerical methods for fluid dynamics. Springer, Berlin; 1997.

[41] Spinewine B, Zech Y. Small-scale laboratory dam-break waves on movable beds. J Hydraul Res 2007;45:73–86.

[42] Dressler RF. Comparison of theories and experiments for the hydraulic dam-break wave. Int Assoc Sci Hydrology 1954;3:319–328.

[43] Bellal M, Iervolino M, Zech Y. Knickpoint migration process: experimental and numerical approaches. Proc, 12th Conf on "Sediment and Sedimentation Particles" Prague, Czech Republic 2004;:–.

[44] Tingsanchali T, Chinnarasri C. Numerical modelling of dam failure due to flow overtopping. Hydrological Sciences Journal-Journal des Sciences Hydrologiques 2001;46:113–130. doi:10.1080/02626660109492804.

[45] Palumbo A, Soares-Frazao S, Goutiere L, Pianese D, Zech Y. Proc., River Flow 2008 International Conference on Fluvial hydraulics, Cesme. ; 2008.

[46] Goutiere L, Soares-Frazao S, Zech Y. Dam-break flow on mobile bed in abruptly widening channel: experimental data. J Hydraul Res 2011;49(3):367–371. doi:10.1080/00221686.2010.548969.

[47] Bilanceri M, Beux F, Elmahi L, Guillard H, Salvetti M. Linearized implicit time advancing and defect correction applied to sediment transport simulations. Comp Fluids 2012;63:82–104. doi:10.1016/j.compfluid.2012.04.009.